Structure and fracture resistance of alligator gar (*Atractosteus spatula*) armored fish scales

Wen Yang [a], Bernd Gludovatz [b], Elizabeth A. Zimmermann [b], Hrishikesh A. Bale [c], Robert O. Ritchie [b,c,*], Marc A. Meyers [a,d,e]

[a] Materials Science and Engineering Program, University of California, San Diego, La Jolla, CA 92093, USA
[b] Materials Sciences Division, Lawrence Berkeley National Laboratory, Berkeley, CA 94720, USA
[c] Department of Materials Science and Engineering, University of California, Berkeley, CA 94720, USA
[d] Department of Mechanical and Aerospace Engineering, University of California, San Diego, La Jolla, CA 92093, USA
[e] Department of NanoEngineering, University of California, San Diego, La Jolla, CA 92093, USA

ARTICLE INFO

ABSTRACT

The alligator gar is a large fish with flexible armor consisting of ganoid scales. These scales contain a thin layer of ganoine (microhardness ∼2.5 GPa) and a bony body (microhardness ∼400 MPa), with jagged edges that provide effective protection against predators. We describe here the structure of both ganoine and bony foundation and characterize the mechanical properties and fracture mechanisms. The bony foundation is characterized by two components: a mineralized matrix and parallel arrays of tubules, most of which contain collagen fibers. The spacing of the empty tubules is ∼60 μm; the spacing of those filled with collagen fibers is ∼7 μm. Using micromechanical testing of such scales in a variable-pressure scanning electron microscope, we identify interactions between propagating cracks and the microstructure, and show that the toughness of the scales increases with crack extension in a classical resistance-curve response from the activation of extrinsic toughening mechanisms. We demonstrate how mechanical damage evolves in these structures, and further identify that the reinforcement of the mineral by the network of collagen fibers is the principal toughening mechanism resisting such damage. Additionally, we define the anisotropy of the toughness of the scales and relate this to the collagen fiber orientation.

Published by Elsevier Ltd. on behalf of Acta Materialia Inc.

1. Introduction

Fish scales are lightweight flexible dermal armor. They characteristically overlap; besides protection, this imbrication can also provide flexibility so that the fish can flex their bodies in different ways (including bending and twisting) for predation, defense and mobility. Three parameters describe the geometrical characteristics of scales [1]: aspect ratio (=total length/thickness); degree of imbrication (=exposed length/total length) and the angle of scales with the surface plane. The scales contribute only ∼1–5% of the fish's body weight and are classified into ganoid, elasmoid, placoid, cycloid and ctenoid; each class has a distinct structure and mechanical performance [2–8]. Protection mechanisms against predation by other fish have been studied recently for *Polypterus senegalus* [3], *Arapaima gigas* [4] and *Morone saxatilis* [5].

For example, the elasmoid scale of *A. gigas* has a highly mineralized external layer, which is hard and stiff, and an inner collagen

layer with a laminate structure where the modulus is a factor of two or more lower [9–11]. The collagen components in the laminate structure of the inner layer undergo stretching and sliding under tensile loads, thereby resisting fracture. Similarly, the ctenoid scale of striped bass (*M. saxatilis*) also has two layers: a bony layer and a collagen layer [5].

The ganoid scale of *P. senegalus* has four layers: ganoine (outer layer), dentin, isopedine and bone (inner layer) [12]. The ganoine layer is highly mineralized, containing ∼95 vol.% hydroxyapatite (HAP) nanocrystals [13,14], typically ∼220 nm in length and ∼40 nm in width, whose long axis is oriented perpendicular to the surface of ganoine [15], and less than 5% organic [13]. Beneath the outer ganoine layer, the mineralization decreases from the dentin layer to the bone layer with the hardness H and elastic modulus E decreasing from ∼1.2 GPa (dentin) to ∼0.5 GPa (bone) and from ∼29 GPa to ∼17 GPa, respectively [12].

In this paper we examine the scales of the large freshwater fish, the alligator gar (*Atractosteus spatula*). We present the first systematic study of their structure via synchrotron X-ray computed tomography and high-resolution scanning electron microscopy. Additionally, we investigate the mechanical response of the scale

---

* Corresponding author at: Department of Materials Science and Engineering, University of California, Berkeley, CA 94720, USA. Tel.: +1 510 486 5798.

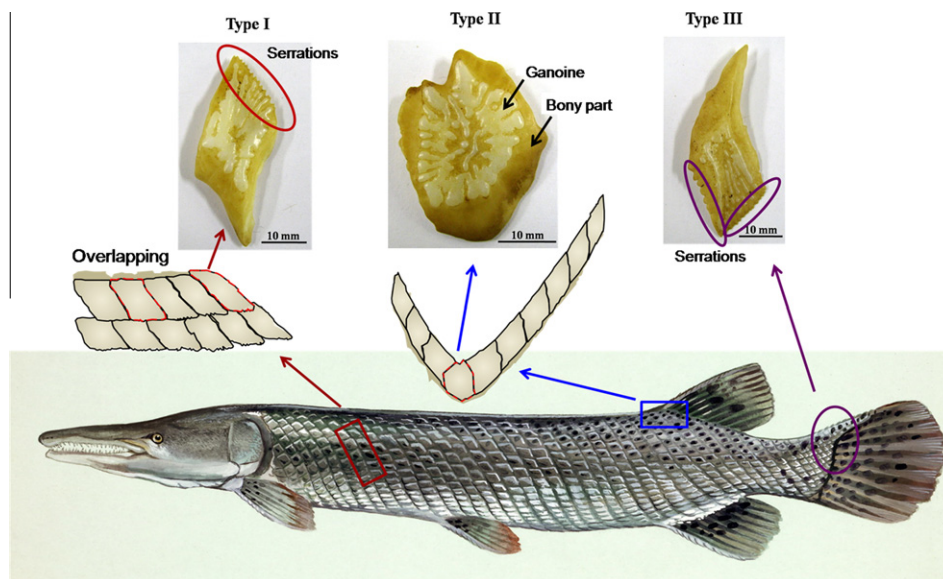*E-mail addresses:* RORitchie@lbl.gov, ritchie@berkeley.edu (R.O. Ritchie).

Fig. 1. Alligator gar: different types of scales located in different parts of body. Type I is the common scale, of rhombic shape and with one serrated edge; types II and III, at junctions and extremities, are scales without any serrations and two serrated sides, respectively.

with emphasis on its uniaxial tension/compression behavior and crack propagation resistance as a basis for its function of an effective natural armor.

The gar is one of the largest freshwater fish in North America (they can also survive in brackish water and saltwater); average weights are in the range of 50–60 kg but large gars may reach 150 kg in weight and 3 m in length. As shown in Fig. 1, it is characterized by a long cylindrical body covered with hard scales that have different shapes. Due to the different aspect ratios and geometric requirements on the armor of alligator gar, there are three types of scales, which we term types I, II and III in Fig. 1. Most scales are type I, having an approximately regular rhombic shape with one serrated edge and overlap in a regular pattern forming inclined rows on the fish body.[1] The aspect ratio is characteristically equal to 8.66 and the degree of imbrication is 0.78, which permits flexibility of movement for the fish.

The scales (classified as ganoid) have two distinct layers: the white external layer consists of ganoine and the internal yellow layer has a bony structure. The ganoine does not cover the bone completely, only ~40–70% of its surface. This is due to two reasons: the unserrated edges of the scales overlap by ~30% (imbrication) and are thinner; the ganoine is irregular and has ridges and gaps. The bony parts remain exposed (shaped as pits and grooves) in the center of the ganoine region. Despite the absence of dentin and isopedine layers, the hardness and modulus (obtained by nanoindentation) of ganoine ($H \sim 3.6$ GPa, $E \sim 71$ GPa) and bone ($H \sim 0.7$ GPa, $E \sim 21$ GPa) are close to those of the ganoine scale from *P. senegalus* [16]. The scales overlap in a pattern in which the white serrated edge (shown by the ellipses in Fig. 1) is on top of the yellow bony part on the opposite side of the adjoining scale. The thickness of the bony part decreases close to the edge of the scale to allow for the overlap, ensuring constant total thickness of the protective armor.

2. Experimental procedures

2.1. Materials

For the present study, alligator gar scales were received from Dianne Ulery (http://www.ccss.us/index.html). They were taken from an adult gar and were obtained with both the ganoine and bony layers intact. The maximum thickness measured at the center of the complete scales was ~4.5 to 5 mm and the length measured along the rhombus' long diagonal was ~30 to 40 mm.

2.2. Sample preparation, mechanical testing and characterization procedures

The scales were characterized using scanning electron microscopy (SEM) and X-ray computed micro-tomography (CT). In addition, mechanical property measurements were performed to establish the hardness, tensile and compressive responses as well as the fracture toughness in terms of full crack-resistance curves (i.e., R-curves).[2] These measurements were performed on dry as well as wet scales as alligator gars can breathe air and survive above water for several hours.

Specimens for structural characterization were examined in a FEI SFEG ultra-high-resolution scanning electron microscope (FEI, Hillsboro, OR). These samples were sputtered with iridium prior to observation.

2.2.1. Microhardness

Sections of the scale were cut in two orientations to determine the hardness variation from outer layer to inner layer (orientations 1 and 2 shown in Fig. 2c). They were prepared by first sanding with 180# to 4000# silicon carbide papers and then polishing with 0.3 μm and 0.05 μm alumina powder to ensure smooth surfaces. Hardness tests were carried out in dry condition using a Vickers

---

[1] Only a few scales are shaped as type II and type III. Type II scales have a low aspect ratio without serrated edges; they are located at the junction of two orientations of type I scales. Type III scales usually appear at the extremity of the alligator gar armor. They have two serrated edges, the other scale direction resembling a tooth-like peg with no serrated edges.

[2] The crack-resistance, or R-curve provides an assessment of the fracture toughness in the presence of subcritical crack growth. It involves measurements of the crack-driving force, e.g., the stress intensity K, strain-energy release rate G or J-integral, as a function of crack extension (Δa). The value of the driving force at $\Delta a \rightarrow 0$ provides a measure of the crack-initiation toughness whereas the slope and/or the maximum value of the R-curve can be used to characterize the crack-growth toughness.
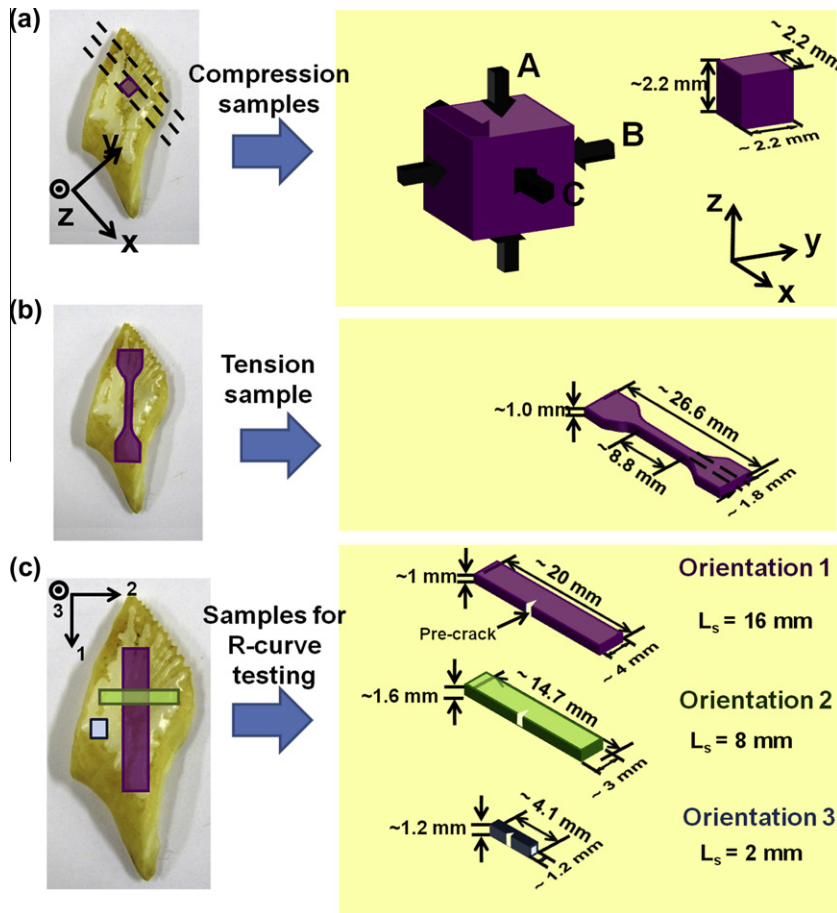
Fig. 2. Dimensions, shapes and orientations of specimens for mechanical testing. (a) Compression; orientation A (OZ): loading perpendicular to surface of scale; orientations B (OY) and C (OX): loading in plane of scale. (b) Tension and (c) R-curve testing in three orientations 1, 2 and 3, where L_s is the loading span. (Compression samples (a) were manufactured parallel to the serrated edge in order to obtain the largest number of samples per scale.)

indentation load of 100 g with a LECOM-400-H1 (LECO, Joseph, MI) hardness testing machine with a holding time of 10 s.

2.2.2. Tension/compression tests

As the scales display a complex structure, the mechanical properties were tested in one or three orientations, as outlined in Fig. 2 for the compression, tensile and fracture toughness experiments. Due to the limitation in thickness of the scale and the necessity to have flat and parallel samples, the compression samples were parallelepipeds in shape with a length of ∼2.2 mm. Three loading orientations were used (Fig. 2a): in orientation A loading was applied perpendicularly to the scale's surface, and in orientations B and C loading was aligned with the plane of the scale along the directions indicated in Fig. 2a. Tension samples were prepared in a dog-bone shape as shown in Fig. 2b. They were cut along the long diagonal of the scale with a gauge length of ∼8.8 mm, a thickness of ∼1 mm and a width of ∼1.8 mm (after polishing). After preparation of the compression/tension samples, some were soaked in fresh water for more than three days, so that the wet specimens contain (on average) ∼3.7 wt.% water, while the others were dried in a ventilated room at room temperature with a humidity of ∼78%. The wet samples were tested immediately after taking out of water and all the compression and tension tests were performed in the same condition with a humidity of ∼78%.

All tension and compression specimens were tested in an Instron 3367 testing machine (Instron Corp., Norwich, MA) at a strain rate of $10^{-3} s^{-1}$. Compression samples were tested in two manners: (a) the standard way (compressed until failure in one cycle) and (b) subsequently unloaded and reloaded to evaluate the effect of damage on the reloading curve. The first loading cycles were from 0% to 13%, 0% to 18% and 0% to 25%. The lateral surfaces were examined by SEM to assess the damage in the first cycle. The reloading stage was continued until the failure of the specimens. The time interval between the end of unloading and reloading was less than 3 days. The lateral surfaces of the tension surfaces were also examined by SEM.

2.2.3. Fracture toughness

Fracture toughness samples were prepared for three-point bending testing to measure the R-curve in the three orientations (Fig. 2c). For orientation 1 along the long diagonal of the scale, specimens were ∼20 mm in length with a width and thickness of ∼4 and ∼1 mm, respectively. Samples in orientation 2 were cut along the short diagonal of the scale, with an average length, width and thickness of ∼14.7, ∼3 and ∼1.6 mm, respectively. Samples in orientation 3 were the smallest and cut along the thickness of the scale with a limited length of ∼4.1 mm and a side length of ∼1.2 mm. The loading spans used for three-point bending in the three orientations 1, 2 and 3 were, respectively, 16, 8 and 2 mm. The surfaces of the R-curve samples underwent the same polishing procedure as the microhardness samples. A blunt notch was cut into each sample with a diamond blade and sharpened using a razor blade irrigated in 1 μm water-based diamond suspension.

The resulting micro-notch in each sample had a length approximately half the width of the specimen with a consistently sharp root radius of ~5 μm, thus creating single-edge notched bend SE(B) samples.

Toughness tests were performed under wet and dry conditions; following sample preparation, prior to testing, the wet samples were soaked in water for 12 h and the dry samples air-dried for at least 12 h. Testing was performed using a Gatan Microtest 2 kN bending stage (Gatan, Abingdon, UK) in a Hitachi S-4300SE/N scanning electron microscope (SEM) (Hitachi America, Pleasanton, CA) at 25 °C in variable pressure mode at a vacuum of 35 Pa, with imaging in back-scattered electron mode. Samples were loaded in three-point bending at a displacement rate of 0.55 μm s^{-1}. This setup provides accurate mechanical measurements of the fracture toughness and R-curve with simultaneous imaging in real time of the crack path and its interaction with the microstructural features of the material [17].

The small size of the samples in at least one orientation (orientation 3) required the use of a non-linear fracture mechanics-based approach (i.e., J-integral) to quantify both the elastic and inelastic contributions to the fracture toughness with crack extension.[3] J–R curves for samples in all orientations were determined in general accordance with ASTM Standard E-1820 [18] and subsequently K-based fracture toughness values were back-calculated based on the relationship between K and J for nominally mode-I fracture, where $K_J = (J \cdot E)^{1/2}$. Elastic modulus, E, values were determined for each orientation in both wet and dry conditions from nanoindentation measurements. Polished samples oriented in each condition were indented with a Triboindenter (Hysitron, Minneapolis, MN) equipped with a Berkovich tip. A trapezoidal loading profile was used to indent the samples with a 100 μN s^{-1} loading rate, a peak load of 600 μN and a hold period of 10 s. Ten indents were performed on each sample with a 10 μm spacing. The average modulus values, required for the toughness calculations, for wet samples tested in orientations 1, 2 and 3 were 9.98, 10.01 and 10.04 GPa, respectively, while the corresponding moduli under dry conditions were 13.8, 10.9 and 13.2 GPa.

2.2.4. X-ray computed micro-tomography

Synchrotron X-ray computed micro-tomography was performed at beamline 8.3.2 of the Advanced Light Source synchrotron (ALS, Lawrence Berkeley National Laboratory) to visualize the three-dimensional (3-D) distribution of tubules and the crack paths through the scale after R-curve testing. The setup is similar to the standard tomography procedures [19] in that samples were rotated in precise incremental steps in a monochromatic X-ray beam and the transmitted X-rays imaged via a scintillator and an optics set-up to give an effective voxel size in the reconstructed 3-D image of 0.65 μm. The samples were scanned in absorption mode and the reconstructed images were obtained using a filtered back-projection algorithm. In absorption mode, the gray scale values of the reconstructed image are representative of the absorption coefficient. To maximize the signal to noise ratio and optimize the interaction between the X-rays and the sample, incident X-ray energy of 18 keV was selected with an exposure time of 350 ms. The datasets were reconstructed using the software Octopus (Octopus v8, IIC UGent, Zwijnaarde, Belgium) and 3-D visualization was

performed using Avizo™ software (VSG, Visualization Sciences Group, Inc., Burlington, MA, USA).

3. Structural characterization

3.1. Scanning electron microscopy

Fig. 3a shows the two layers of the gar scale: ganoine and bone with the interface in zigzag pattern shown by the arrows. The ganoine layer is only ~600 μm thick and is highly mineralized, while the thickness of the bony part reaches more than 3 mm. The detailed structural characterization of ganoine is shown in Figs. 3b–d. The polished cross-section shows a dimpled structure which is formed by the different orientations of the mineral rods of calcium-deficient hydroxyapatite, $Ca_5(PO_4)_3(OH)$; these rods align with the edge of the dimples, as indicated by the dashed lines and arrows in Fig. 3b. Fig. 3c shows different orientations of the mineral rods, marked A, B, C and D. It appears that the crystal rods in orientation A form the edge of one pit, while the rods in orientations B, C and D form another dimple. The mineral rods have a thickness of ~40 nm (Fig. 3d).

Fig. 4 shows the microstructure of the bony part. It is much less mineralized than the ganoine and is characterized by tubules and collagen fibers. The compactness decreases from the region adjacent to ganoine (Fig. 4c) to the internal region (Fig. 4d) where more tubules or collagen fibers appear. From the top view of the scale, at least one large diameter tubule can be observed in the center part of the ganoine region where the exposed bony part is shown by the circle in Fig. 4a. Three large diameter tubules (~200 μm) can be observed on this scale (Fig. 4b). In the bony part, tubules (marked by black arrow) and collagen fiber heads (marked by white arrows) can be seen in Fig. 4c. After polishing and partial drying, some of the interfaces between the tubules and collagen fibers separate and create a dark "crescent moon" shape. The spacing of tubules and collagen fibers (from top view) in the bony layer seems to increase from the inside (close to the fish skin, Fig. 4d) to the surface (close to the ganoine, Fig. 4c).

Collagen fibers are embedded in the matrix of the bony layer, and consist of collagen fibril-mineral rods, as shown in Fig. 5b. They are also encased in tubules with a spacing of ~5 μm; the average diameter of the collagen fibers is ~3 μm (Fig. 5b). Fig. 5c shows mineralized collagen fibers at the transition from the tubule to the matrix. The mineral in the matrix forms crystalline rods perpendicular to the mineralized collagen fibers; these collagen fibers are comprised of collagen fibrils with a characteristic diameter of ~100 nm and displaying the characteristic 67 nm periodicity of the mineral (Fig. 5d). The diameter of these fibrils is consistent with reports on connective tissue (rat-tail tendon: 40 nm; rabbit tendon: 100 nm; horse: 200–500 nm [20]). The average diameter of the fibers measured in the scale (~3 μm) is typical for collagen in most biological materials (e.g. 1–4 μm [21]). Figs. 5b–c also show the matrix material; features are perpendicular to the tubule axis and it is thought that they consist of a collagen fibril–mineral rod mixture. Fig. 6a shows features (dashed lines) whose spacing is consistent with the tubules; their orientation varies from the inside to the outside of the layer, where they are approximately perpendicular to the growth lines. Upon closer examination by SEM (Fig. 6b), one can see that the collagen fibers are not straight, with changes in the curvature showing that the collagen is somewhat irregularly aligned throughout the thickness of the scale; they clearly bend, which presumably results from the scale growth process.

It is also possible that the hollow tubules originally contain collagen that is leached out as the scale grows. As the scale grows, assuming that it is geometrically self-similar, the collagen fiber

---

[3] Assuming a crack-initiation toughness, K_i, of 2 MPa m$^{1/2}$ and a yield strength, σ_y, of 100 MPa, a minimum sample thickness of 1 mm is required for plane strain conditions. Given a small plastic zone compared to all other sample dimensions (small-scale yielding) additionally allowed for K-controlled fracture in orientations 1 and 2 whereas the size of samples in orientation 3 fulfilled validity criteria for J-controlled testing conditions. Accordingly, tests in all orientations were carried out in plane strain using a non-linear elastic fracture mechanics-based approach in terms of the J-integral.
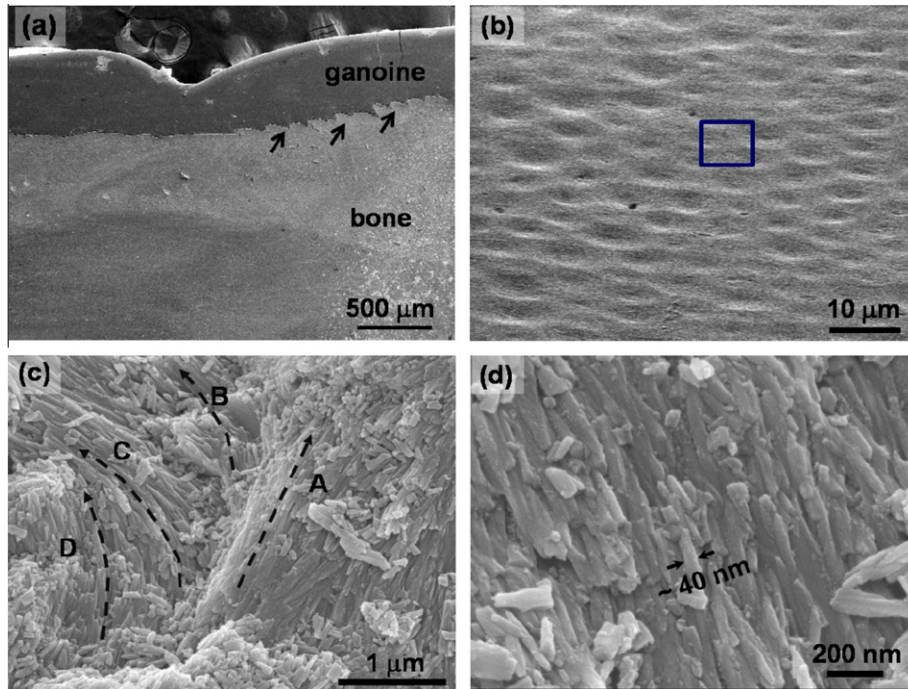
Fig. 3. Structural characterization of ganoine in the gar scale: (a) cross-section showing both the ganoine and bone layers of the scale with the zigzag-pattern interface (arrows), (b) dimpled appearance of polished section, (c) higher magnification of box in (b) showing mineral crystals with different orientations: A, B, C and D, (d) parallel mineral crystals with diameter ~40 nm.
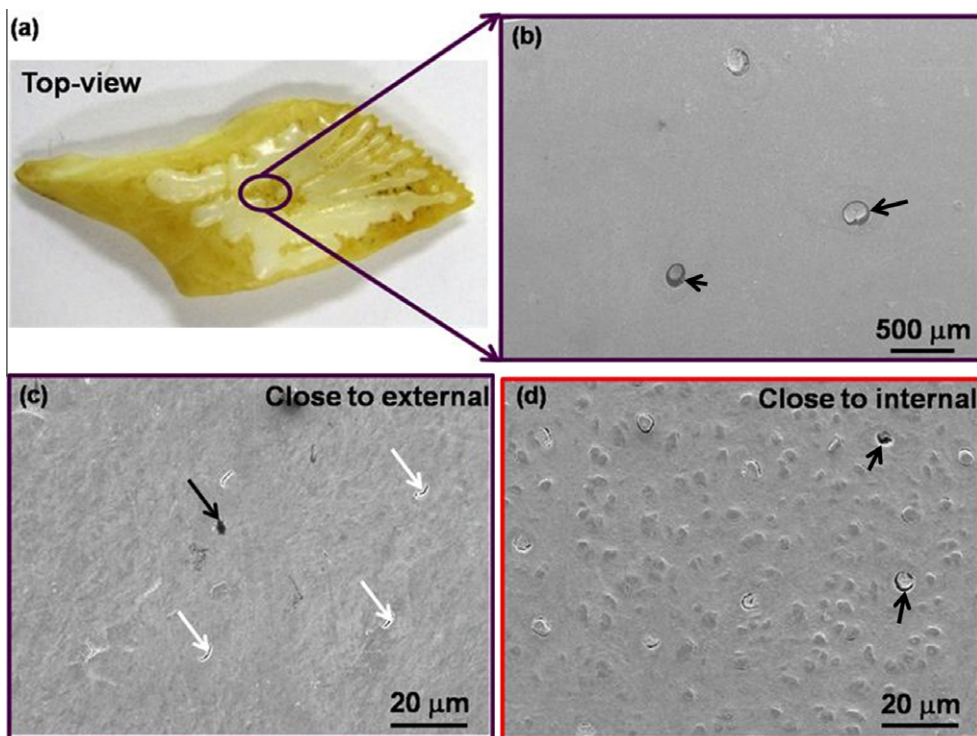

Fig. 4. Type I scale: (a) top view of entire scale with white ganoine as the external layer and internal yellow bony layer, (b) large tubules on the exposed bony part in the center of the ganoine, (c) sparse tubules (black arrow) and collagen fiber heads (white arrows) in bony layer close to ganoine, (d) densely populated collagen fiber heads in bony layer close to internal region. Note the separation of some collagen fibers from the tubules (black circles pointed out by arrows in (b) and (d)).

growth shows irregularities that are caused by fluctuations of temperature, seasons or food. It is feasible that the collagen fibers reduce their growth process seasonally or that the mineral grows faster at the head of the collagen fibers and impede their growth. For this reason, one cannot observe collagen fibers propagating through the entire thickness of the scale.
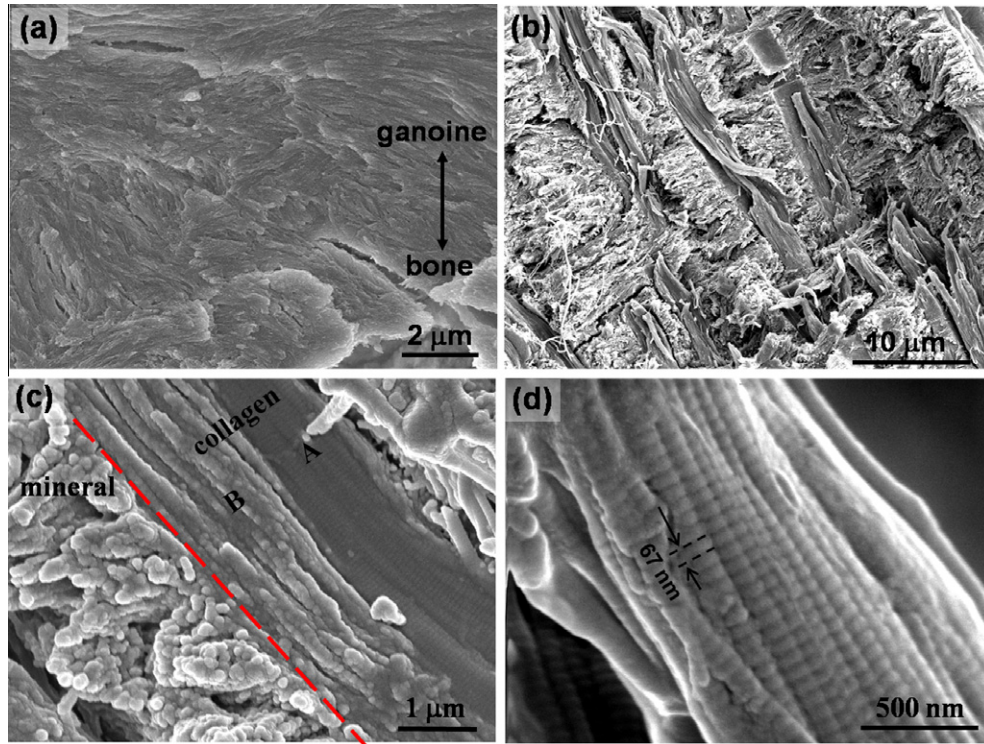
Fig. 5. Structural characterization of the bony part of the scale: (a) region in bony part close to interface with ganoine showing the decreasing compactness from ganoine to bone, (b) aligned ruptured collagen fibers (~3 μm diameter) exposed in fracture surface, (c) closer view of collagen fiber region, with collagen fibers in region B being more mineralized than region A and adjacent mineral possibly containing mineralized collagen fibrils, (d) mineralized collagen fiber showing fibrils (~100 nm diameter) with the characteristic 67 nm periodicity due to the spacing of the mineral.
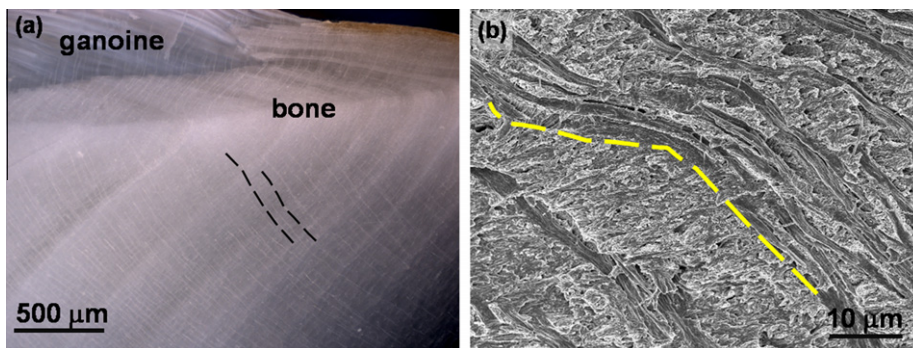
Fig. 6. (a) Optical micrograph showing interface between ganoine and bony part (on top) and white lines in bone, two of which are marked with dashed lines; these are tubules, spaced ~50 μm. Their angle with surface varies because of curvature, (b) SEM micrograph showing curved trajectory of collagen fibers in the bony layer.

The diameters and separation of the collagen fibers and tubules near the inner layer are shown in Fig. 7. The collagen fibers (with diameter of ~3.1 μm and spacing of ~7.2 μm) appear much closer to each other than the tubules (diameter of ~6.5 μm and spacing of ~62 μm). The empty tubules have approximately twice the diameter of the collagen fibers.

3.2. X-ray computed micro-tomography

The alignment and orientation of the tubules in the alligator gar scale can be revealed in three dimensions using synchrotron X-ray computed micro-tomography (Fig. 8). The tubules are almost parallel to each other and have lengths reaching 100 μm through the thickness of the scale. The spacing between them (~30–60 μm) is characteristic of the empty tubules. Individual collagen fibers are not visible with tomography because the contrast mechanism is based on how the structure absorbs the X-rays; as the collagen fibers have a similar density to the surrounding matrix, the two structural features are indistinguishable. Although individual collagen fibers are not visible with the spatial resolution of this technique, it is clear that the empty tubules are roughly perpendicular to the surface of the scale but their orientations vary with an angle of roughly 8–15° from the z-axis to both the x and y directions (these orientations are defined in Fig. 8). However, the region imaged is small (~200 μm) and there is a definite possibility that these tubules reorient themselves through the cross-section, as suggested in Fig. 6.
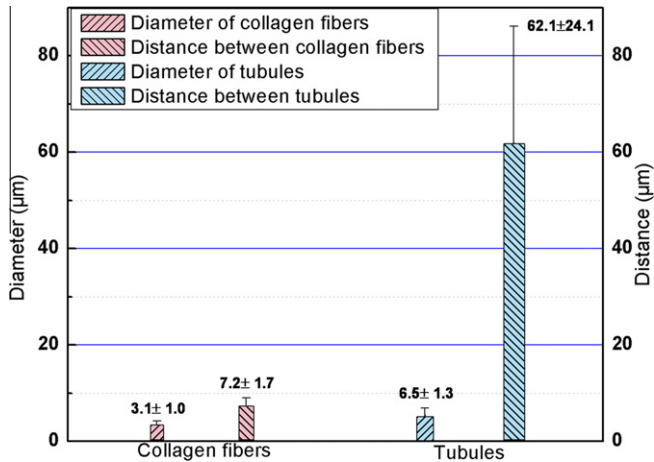
Fig. 7. Diameter of, and distance between, the collagen fibers and tubules in the bony layer (at the bottom of the scale close to the fish skin). Measurements were made on plane parallel to surface of scale (orientation A (OZ) shown in Fig. 2a).

Fig. 9. Hardness in transverse and longitudinal cross-sections of the alligator gar scale with the representative indentations in the ganoine and bony layer under load of 100 g. The distance is normalized to the thickness of scale: ~4.3 mm. (At this scale, the error bars for the bony part are smaller than the size of the data points.)

4. Mechanical behavior and fracture mechanisms

4.1. Hardness

Due to the differences in composition and structure of the ganoine and bony parts, the hardness of the two layers is quite different. Fig. 9 shows the Vickers indentations in the ganoine and bony part of the scale after loading to 100 g; the size of the indentation in the inner layer was ~2.5 times of that in the ganoine. Scans of the microindentation hardness along the cross-section in both the transver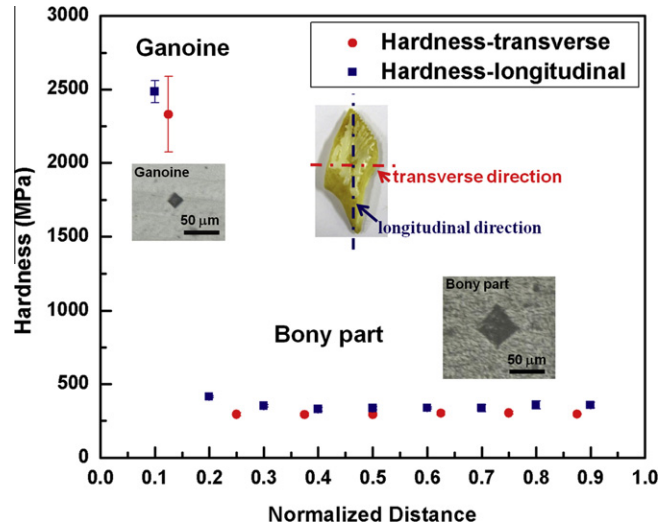se (short diagonal of the scale) and longitudinal directions (long diagonal of the scale), shown in Fig. 9, reveal that the ganoine layer (~2.5 GPa) is about six times harder than the bony part (~0.4 GPa). This is because the ganoine layer is far more mineralized than the bony part, which contains a significant concentration of the softer collagen fibers. The hardness of the entire bony layer appears to be essentially constant. It is possible that there is a gradient between the ganoine and bony layer; however, based on the nanoindentation study conducted earlier [16], no
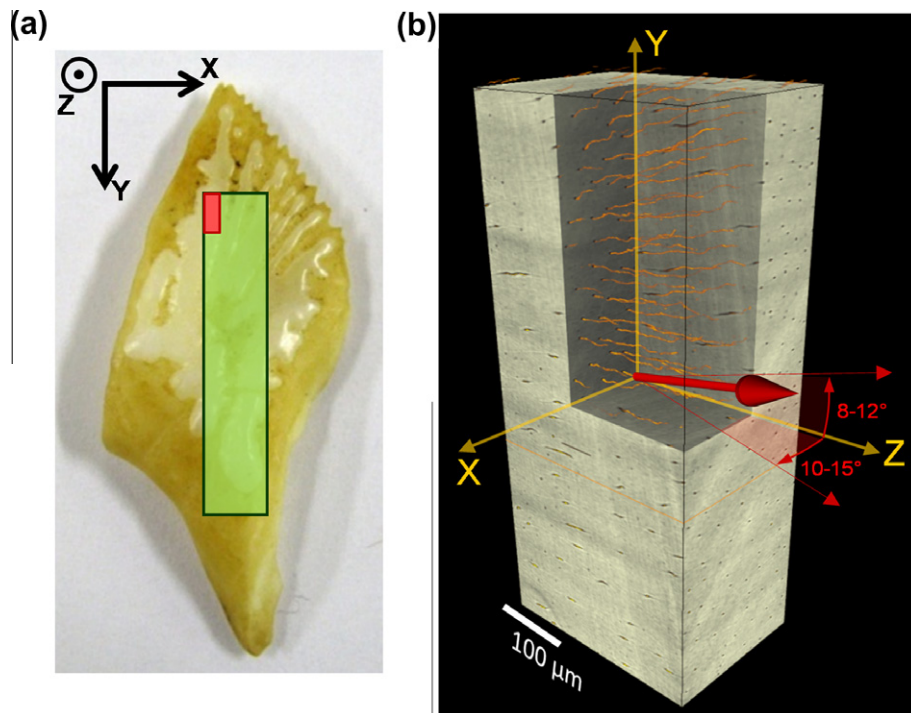

Fig. 8. Synchrotron X-ray computed micro-tomography of alligator gar scales shows the underlying orientation of the tubules. (a) Optical image of the sample used for tomography (indicated by red small rectangle) was extracted from a fracture toughness specimen (green large rectangle) along the length of the scale. (b) Perspective 3-D view derived from the tomography data: here, the z-axis is normal to the outer surface of the scale, while the y- and x-axes follow the length and width of the scale, respectively. The tubules are colored orange represented by wavy lines in the upper quadrant of the reconstruction and the large red arrow shows their average orientation with respect to the z-axis.
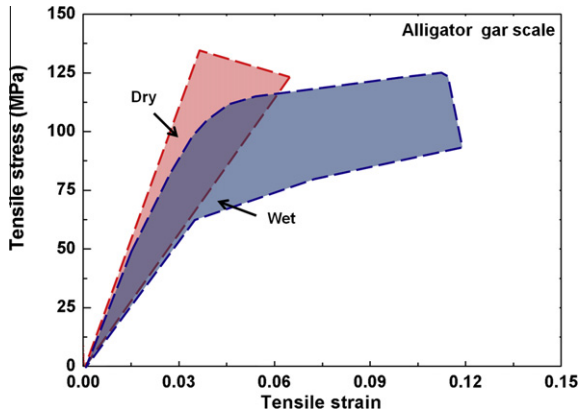
Fig. 10. Range of tensile stress–strain curves of wet (eight specimens) and dry (20 specimens) alligator gar scale samples tested along the longitudinal axis (see Fig. 2b) represented by scatter bands. Note the bilinear response of wet specimens, which indicates some degree of "plasticity", which is clearly distinguishable from linear response of dry specimens, which are more brittle and deform largely elastically.

clear gradient was found between the two layers. SEM observation shows that there is a gradient in density between the ganoine and bony layer, and it is clear that the number of collagen fibers decreases in the bony layer from the ganoine layer to the internal boundary, as shown in Fig. 4c-d. From Fig. 6a, one can distinguish an "intermediate layer", which is caused by the orientation change of the growth lines. Thus, the possibility of a gradient cannot be excluded. However, the change in hardness throughout the scale is consistent with its function; the highly mineralized ganoine has a high hardness to protect the fish from penetration by teeth, whereas the bony part with collagen fibers provides the toughness

and prevents fracture of the scale. The scale has the important function of redistributing the load over a larger surface, as has been recently shown by Vernerey and Barthelat [22].

4.2. Tensile constitutive behavior

Fig. 10 shows the range of uniaxial stress–strain tensile curves for wet and dry alligator gar scales (bony part). It is clear that the linear mechanical response of dry scales implies primarily elastic deformation behavior; the bilinear response of wet scales displays evidence of significant "plasticity" due to the hydrated condition of the collagen fibers. However, although the dry scales lack much post-yield plastic deformation, the average toughness of the wet and dry scales are not too different, at least when assessed, in terms of the areas under the stress–strain curves.

Mechanistically, the evidence of "plastic deformation" in wet scales, as compared to the nominally purely elastic behavior of dry scales, can be attributed to the formation of hydrogen cross-linking between the collagen and water molecules. Similar to behavior in tooth dentin [23], in the dry state, hydrogen cross-link bonds form directly between the collagen molecules, thereby limiting the process of fibrillar sliding as the prevailing "plasticity" mechanism and sometimes even increasing the stiffness of the tissue. The presence of water, conversely, acts as a "plasticizer" since these hydrogen bonds now form between the collagen and water molecules; the resulting ease of fibrillar sliding of the collagen gives rise to "plasticity" in the tissue and hence some measure of ductility. Molecular dynamics calculations by Gautieri et al. [24] corroborate this effect of hydration on the mechanical response of collagen.

Fig. 11 shows the side view of the scales after the tension tests. For the dry scale, a crack can be seen to propagate through the large-diameter tubule in the center of the scale circled in Fig. 11a; on the other hand, the crack propagates partially around
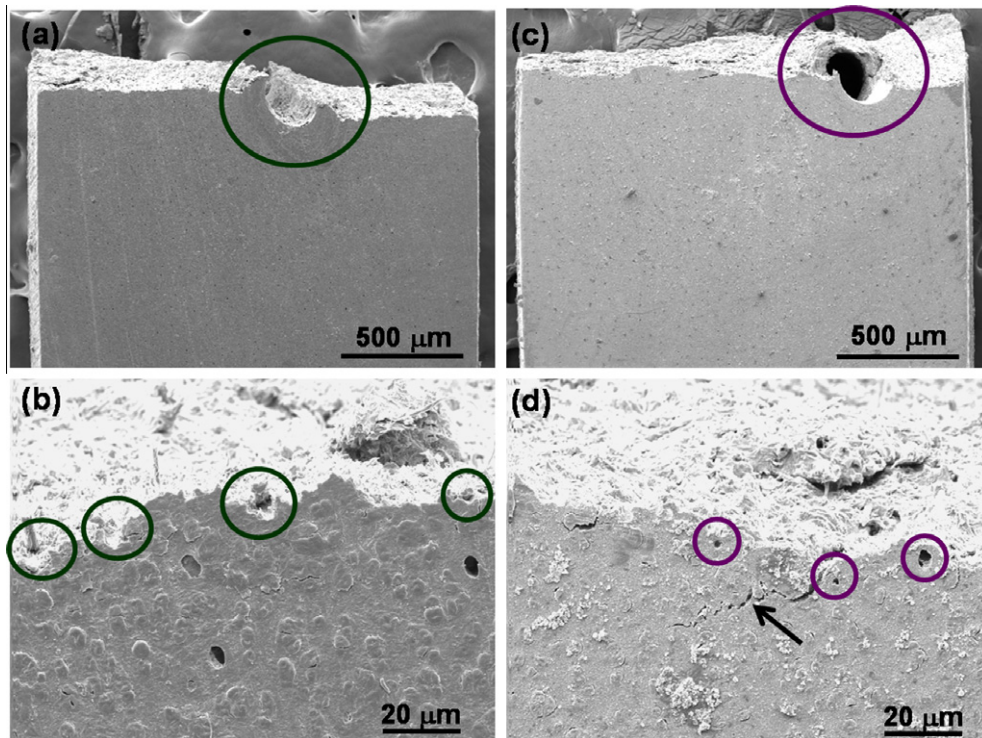

Fig. 11. Side view of the (a and b) dry and (c and d) wet scales after failure in tensile tests; in dry scales, the crack propagates through (a) the large tubule in the center of the scale and (b) the micro-tubules, in wet scales, the crack propagates partially around (c) the large tubule and (d) the micro-tubules.
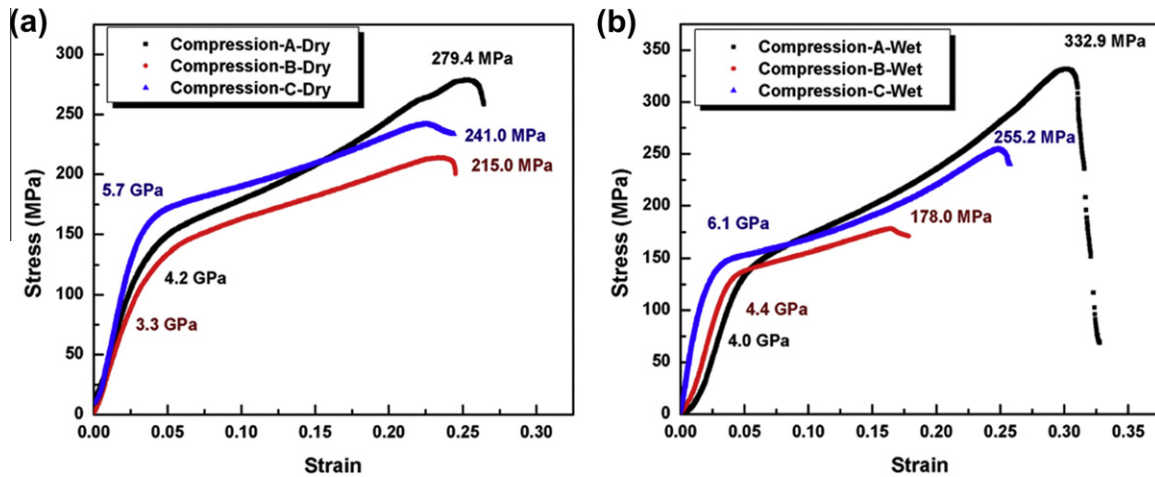
Fig. 12. Typical stress–strain plots of (a) dry and (b) wet specimens tested in compression. Data were obtained by loading in three orientations as defined in Fig. 2(a): A (OZ) – perpendicular to plane of scale; B (OY) and C (OX) – in-plane loading.

Table 1
Compression strengths in orientations A, B and C (ave ± std).

Strength (MPa)	Orientation A	Orientation B	Orientation C
Dry	284.9 ± 42.0	210.1 ± 28.4	240.0 ± 21.9
Wet	312.3 ± 34.8	198.5 ± 30.8	240.7 ± 31.6

the big tubule in the wet scale shown in Fig. 11c. Indeed, at high magnification, the crack propagates through both the tubules and the mineralized collagen fibers in dry scale. The dry mineralized collagen fibers are stiffer and less plastic. The tubules can be considered as voids; as cracks will always follow the lower modulus (more compliant) phase, the crack tends to propagate through these features. Thus, the dry scale retains its toughness through the resulting deflected crack path as well as the energy dissipation from the interaction between the crack and the voids. Conversely, in the wet scales the main crack and secondary cracks tend to avoid the tubules, as shown in Fig. 11d. Thus, although toughening from the meandering nature of the crack path is diminished in the wet scales, the water provides a degree of plasticity in the collagen fibers, leading to somewhat enhanced ductility.

4.3. Compressive response and anisotropy

The compression tests were conducted in three orientations (defined in Fig. 2a) to determine whether the anisotropy of the structure (tubules and collagen fibers) affected the strength. Representative results are shown in Fig. 12.

The mean compressive strengths, and their standard deviations, are shown in Table 1, where it is clear that there is a significant effect of orientation on strength. The mean compressive strengths in orientation A for both dry and wet specimens (285 and 312 MPa, respectively) were higher than those in orientations B (210 and 199 MPa, respectively) and C (240 and 241 MPa, respectively). Thus, orientation A has the highest compressive strength, while the difference between strengths of orientations B and C is less clear; this is directly related to the orientation of the tubules.

The compressive strengths of the wet scales in orientations B and C are lower than those of the dry scales, which is consistent with the behavior of hydrated biological materials [2,25,26]; however, in orientation A the effect is reversed, with the wet scales showing a higher compressive strength.
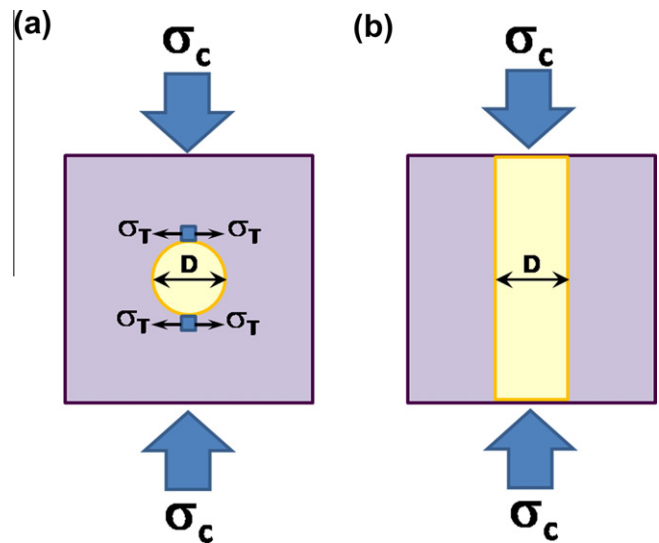

Fig. 13. Schematic arrangement of tubules in compression testing: (a) loading in plane of scale with generation of tensile stresses at top and bottom of tubules (orientations B and C); (b) loading perpendicular to scale surface.

With respect to the structural characteristics in orientation A, the tubules are aligned more closely with the loading direction, whereas in orientations B and C the tubules are perpendicular to the loading direction. The highest strength of orientation A can be explained by the schematic drawing in Fig. 13. The stress concentration generated by the loading of a body with a cylindrical void can be shown [27] to be numerically equal but opposite to the compressive stress:

$$\sigma_T = -\sigma_C \tag{1}$$

This geometry is shown in Fig. 13a. For tubules which are more closely aligned with the loading direction (Fig. 13b), this stress concentration is absent and the failure stress is higher.

To understand the progression of deformation, "plasticity" and damage of the structure, compression tests were conducted by unloading at prescribed strains (13%, 18% and 25%) and subsequently reloading (Fig. 14). These strains correspond to a significant deviation from elastic loading and as such result in
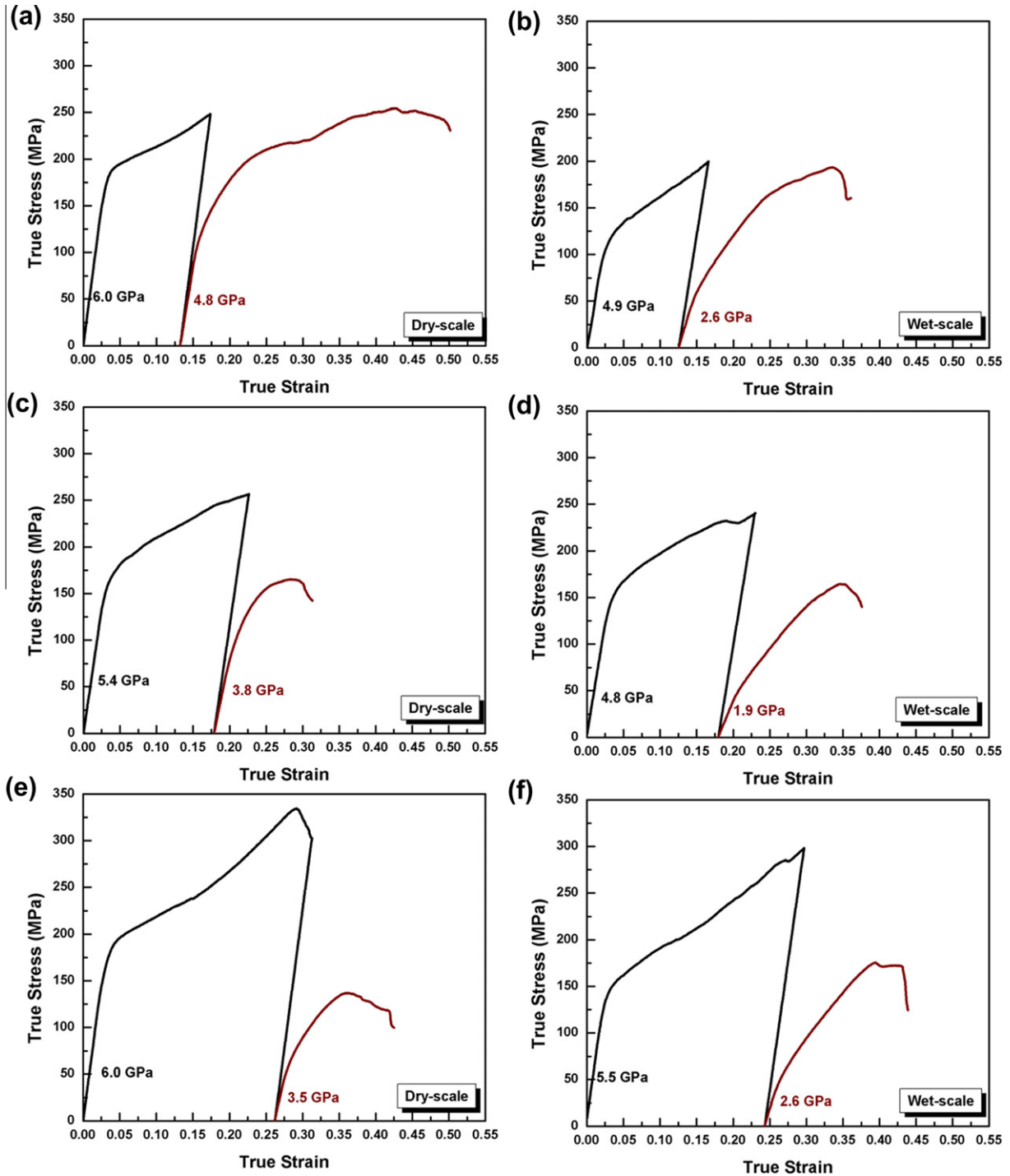
Fig. 14. Compression tests (loading–unloading–reloading) of dry and wet scales tested with different strains in orientation C (OX) – in-plane loading (see Fig. 2a), shown in parentheses from (a to f) in preloading procedure: (a) dry scale (0–13%), (b) wet scale (0–13%), (c) dry scale (0–18%), (d) wet scale (0–18%), (e) dry scale (0–25%), (f) wet scale (0–25%).

significant post-yield deformation. The reloading curves show considerable deviation from elastic response at stresses significantly below the unloading strength, which is evidence of damage accumulation in the structure. As the strain at unloading increases, the reloading strength decreases, showing that damage is gradually increasing. However, the structure still has considerable load-bearing ability up to high strains, demonstrating that there is a significant contribution from "plasticity" in the deformation. The dry specimens show a slightly greater deterioration in strength

by virtue of their enhanced brittleness. If the response were truly plastic, the yield stress would reach the level at the first loading.

The nature of damage generated in the first loading cycle could be assessed by the observation of the lateral surfaces, which exhibited cracks generated in the structure (Fig. 15). Both the wet and dry specimens exhibited shear cracks during compression, which propagated along the collagen direction in the dry scales (shown by the circles in Fig. 15a and the arrow in Fig. 15b) and around the collagen fibers and tubules in the wet scales. In the wet
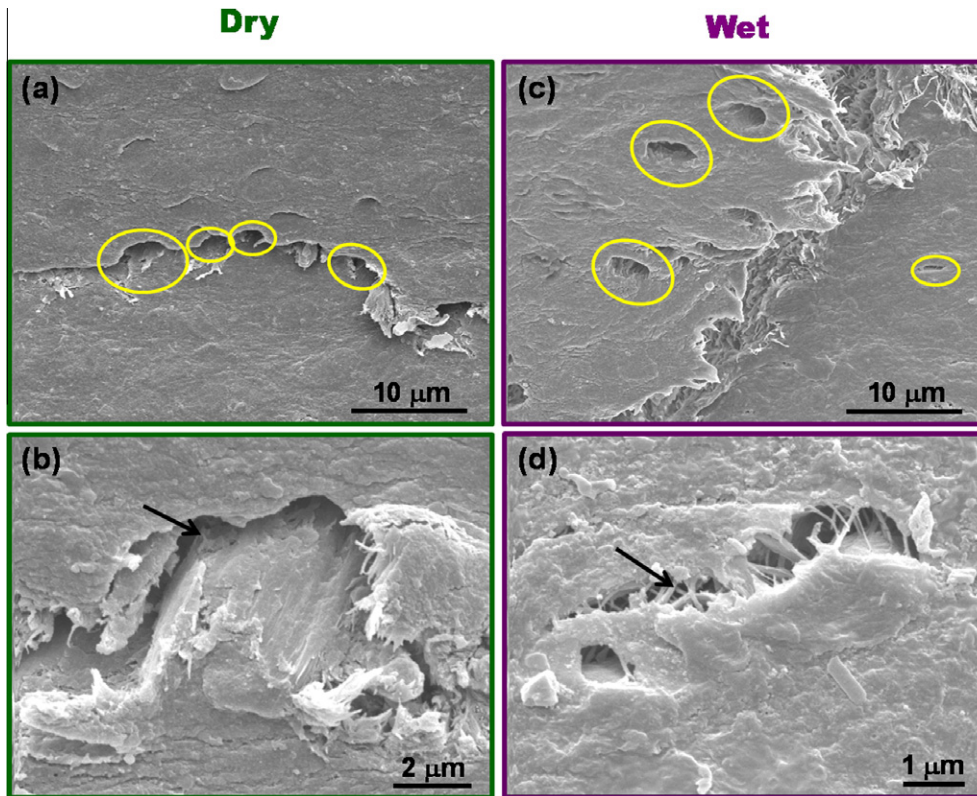
Fig. 15. Damaged structure of dry (a and b) and wet (c and d) scales after the first compression cycle; Note that in (a and b), a shear crack propagates along collagen fibers and tubules, while in (c) the shear crack propagates around the compressed fibers and tubules; (d) ligaments between the mineral and collagen fibers can be seen to resist crack propagation via a crack bridging mechanism.
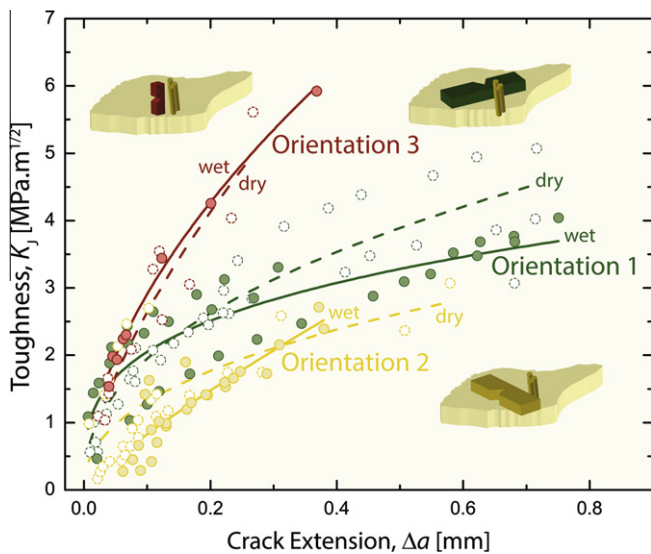

Fig. 16. Fracture toughness crack-resistance curves (R-curves) of alligator gar scales tested on notched three-point bending samples in the environmental scanning electron microscope. The resulting R-curves show the fracture resistance in terms of the fracture toughness, K_J, as a function of crack extension, Δa. Testing of the scales was performed with the crack oriented in three different directions with respect to the scale's microstructure (defined in Fig. 2c and here by the schematics with the tubules drawn as rods). The scales were tested under both dry and wet conditions.

specimens, the tubules were deformed by the compressive stresses from a circular to an elliptical shape.

4.4. Resistance-curve behavior and in situ crack-growth observation

A necessary property of alligator gar scale as a dermal armor is the fracture toughness, which defines its resistance to flaw-like damage and the consequent unstable propagation of cracks. Crack-resistance curve (R-curve) testing was performed along three different orientations in the dry and wet conditions to determine the resistance to the fracture of alligator gar scale, as a function of the initiation and growth of a crack. In situ SEM was used to permit real time imaging of the fracture process and to establish specifically how the propagating cracks interact with the microstructure of the scale. Fig. 16 shows the fracture toughness of the bony part of alligator gar scale tested in three different orientations (defined in Fig. 2c) as a function of crack extension. The slope of the R-curve is a measure of the resistance to crack growth, which is highest in orientation 3. This is strongly dependent on the reaction between the crack propagation and the orientation of both tubules and collagen fibers. In orientations 1 and 2, the tubules and collagen fibers are slightly angled with respect to the crack propagation front. Specifically, in orientation 2 (Fig. 17b), the collagen fibers are mostly in the plane of crack propagation[4] but slightly tilted out of the plane; in orientation 1 (Fig. 17a), conversely, the collagen fibers traverse across the plane of crack propagation, which leads to the small differences in the slope of the R-curve in Fig. 16. In contrast, for orientation 3, the tubules and collagen fibers are oriented nearly

---

[4] In orientation 2, the alignment of the collagen fibers (i.e., the angle between the collagen fibers and the crack front) varies as shown in Fig. 17b and its inset; this variation in alignment is an artifact of the slight variability in the microstructure (i.e., tubules and collagen fibers) throughout the entire scale. Indeed, this variation is also seen on the fracture surface of orientation 1 (Fig. 17a), where the collagen fibers appear generally aligned but with a slightly wavy texture through the scale thickness.
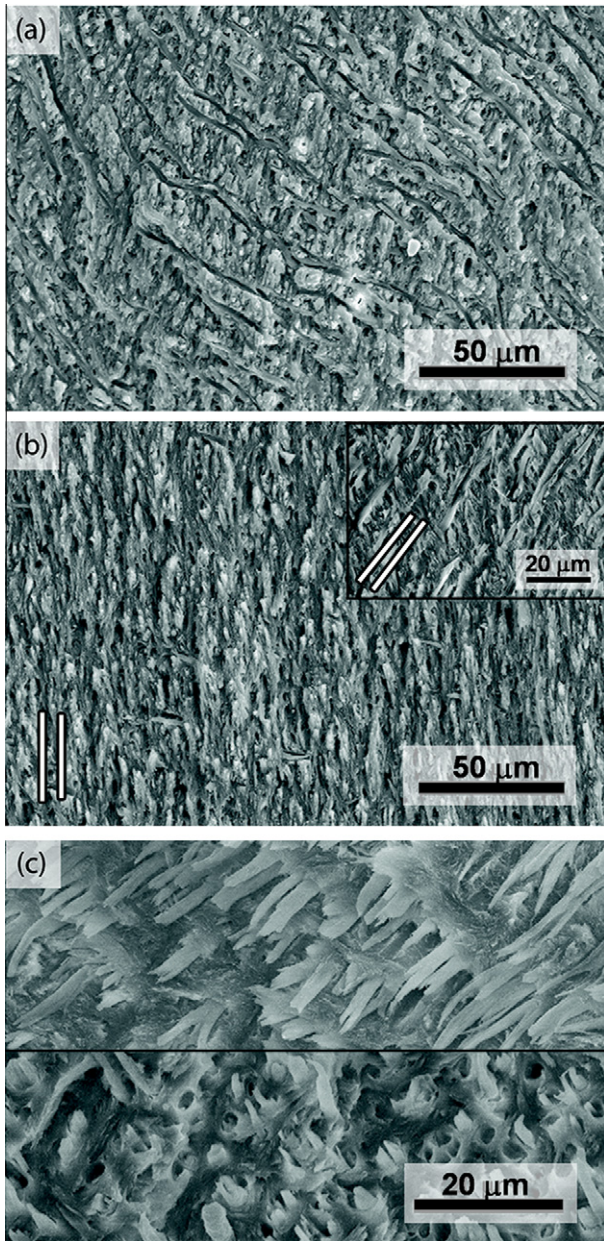
Fig. 17. Scanning electron microscopy images of the fracture surfaces after crack-growth resistance toughness measurements of notched beams in three-point bending, showing the underlying microstructure and its contribution to the toughness. (a) In orientation 1 (Fig. 2c), the collagen fibers traverse from left to right through the scale thickness, consistent with tomography images of the tubule orientation. (b) The collagen fibers in orientation 2 are nearly parallel to the direction of crack growth, but as the inset suggests, there can be some degree of misalignment due to differences in tubule orientation between scales. (c) Orientation 3 has the most favorably aligned collagen fibers, which span the crack wake and in turn contribute to the crack growth resistance; ruptured collagen fibers seen in both pictures.

perpendicular to the orientation of the crack front, which allows the collagen fibers to span the crack wake (Fig. 17c), actively contributing to the crack-growth resistance via a crack bridging mechanism.

Although the different orientations of collagen fibers as well as tubules lead to differences in toughness, the wet and dry conditions for each orientation did not cause significant toughness changes as discussed in Section 4.2 with reference to the uniaxial tensile response (Fig. 10). Due to the potent effect of the fibers spanning the crack wake in orientation 3, differences in the crack propagation resistance in wet vs. dry conditions were not

observed. However, the influence of different hydration conditions on the crack paths became most apparent in orientation 1, where the microstructure has a larger misalignment with the crack propagation front than in orientation 2. The cracks in the dry scale follow the tubules, causing a deflected and twisted crack path, as shown in the 3-D tomography and two-dimensional (2-D) SEM images in Figs. 18a and 19b, respectively, while in the wet scale, the cracks follow a roughly linear path, avoiding most of the tubules and collagen fibers. The tortuosity created by such crack paths in the dry scales can increase the fracture toughness extrinsically by a factor of up to 2 by in-plane deflections and even up to 6 if crack twisting is involved. Similar behavior can be seen in tooth dentin where the crack again follows the dentinal tubules (provided they are not filled with mineral as with aged dentin) [28]. However, under more physically realistic wet conditions, the crack path appears to be unaffected by the presence of the tubules or other smaller features, which provide a source of extrinsic toughening from crack deflection mechanisms in the dry scales. To counter this reduction in extrinsic toughness, wet scales display far more post-yield deformation as indicated in the stress–strain tensile curves shown in Fig. 10. The resulting "plasticity" in the wet material, as described in the above section, enhances the intrinsic toughness by increasing its ductility. Consequently, differences in the toughness between wet and dry scales are not that large and only become apparent as the crack extends where the extrinsic toughening mechanisms become more active.

5. Summary remarks

From this study, it is apparent that the ganoid scales of the alligator gar fish can provide effective protection against predation. Their essential features are the highly mineralized ganoine with its high hardness to protect against penetration, and an underlying bony part containing collagen fibers to provide ductility and toughness to prevent fracture of the scale. The scales are overlapping, which also provides flexibility of movement for the fish [6]. The degree of imbrication of 0.78 is rather low compared to other classes of scales. Indeed, the overlap in elasmoid scales, which are flexible and have much higher aspect ratios (i.e., 25 or higher), is much larger. The ganoid scales have a unique feature, varying thickness so that they fit into each other in a tridimensional pattern.

The gar scales therefore are structurally and geometrically quite different from the elasmoid scales of another large river fish, A. gigas [4], by virtue of the different predators. In the case of the arapaima, the principal predator is the piranha. For the gar, intraspecies predation (larger gar) and alligator require a more robust armor. Interestingly, the scales of P. senegalis [3], also ganoid, provide protection against intraspecies predation. The hard ganoine surface backed by a bony layer with high toughness, as demonstrated here, provides such defense. The thickness of the ganoid scale in the gar (~3.5 mm) is significantly larger than that of the arapaima (~1.5 mm). The hardness of the external layer is three times higher than that of the arapaima [6]. Additionally, the scales have a sharp serrated edge which can effectively inflict damage to the predator. The anisotropy of structure and mechanical properties suggest that the compression of the scale perpendicular to its surface is the most important property, superseding the flexure in importance; the strength is highest in this direction. The extensive plasticity suggests that a damaged scale survives without catastrophic failure upon being compressed during the biting action.

6. Conclusions

During hundreds of millions of years, biological evolution created and adapted scales on fish, reptiles and mammals to form a
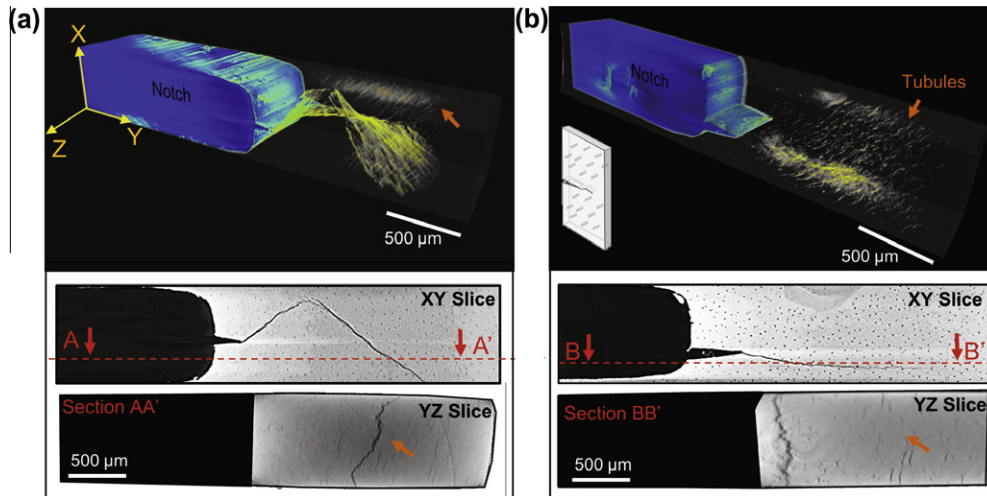
Fig. 18. Synchrotron X-ray computed micro-tomography was used to visualize the crack path in 3-D for the (a) dry and (b) wet alligator gar scales tested in orientation 1 (Fig. 2c). The top image shows tomographs of the path of the crack taking a twisting route through the dry sample's thickness, while the crack in the wet sample propagates relatively straight. (False colors of green define the cracks and blue the pre-crack and notch.) [The bottom images are 2-D slices of the crack path reinforcing the twisted and straight paths, respectively, for dry and wet conditions and blue the pre-crack and notch. The bottom images are 2-D slices of the crack path reinforcing the twisted and straight paths, respectively, for dry and wet conditions.]
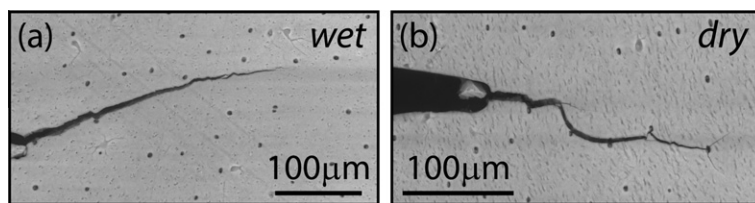

Fig. 19. SEM images of crack paths in orientation 1 shown in Fig. 2c and tested under wet (a) and dry (b) conditions. Whereas in the wet scale the crack path is relatively straight and uninfluenced by microstructural features like tubules and collagen fibers, the crack in dry scale follows the tubules, consistent with Fig. 11.

flexible dermal armor as a protection from attack. In this work, the structure and the mechanical behavior of the scales of the alligator gar fish (*A. spatula*) were investigated with the objective of discerning how individual scales can provide such protection. Our mechanical evaluation of the strength, ductility and toughness of alligator gar scales shows that both the hard ganoine and tough bony part of the scales contribute synergistically to protect the fish. The following specific conclusions can be made:

1. The ganoid alligator gar scale has two layers: a highly mineralized external ganoine and the internal bony layer which is a composite containing collagen fibers and tubules. The main function of ganoine layer is to establish a high hardness barrier against perforation by teeth whereas the bony layer provides a foundation with much greater toughness and impedes cracks in the ganoine to propagate through the scale. The hardness of ganoine is six times higher than the softer bony layer.
2. The bilinear uniaxial stress–strain response of wet scales in both tension and compression can be associated with the presence of significant "plasticity" in the collagen; in contrast, dry scales display a linear stress–strain response with little evidence of such post-yield "plastic deformation" and resultant ductility. This plasticity is enabled by the load transfer from the mineral to the collagen fibers; similar to tooth dentin, in hydrated scales hydrogen bonding occurs between the collagen and the water molecules, the latter acting as a plasticizer, whereas in the absence of water such hydrogen bonding occurs directly between the collagen molecules, thereby restricting fibrillar sliding and hence plasticity in the collagen.

3. Under load, the cracks tend to interact with tubules and collagen fibers embedded within the mineral structure. Highest resistance to cracking is achieved where cracks extend through the thickness of the scale parallel to the surface. Here the tubules and collagen fibers are oriented nearly perpendicular to the orientation of the crack front, allowing the collagen fibers to span the crack wake, actively contributing to the crack-growth resistance via crack bridging.
4. For the other orientations, in dry scales, cracks tend to propagate microstructurally through the tubules and collagen fibers, and the mineralized collagen fibers undergo separation or delamination, whereas in wet scales, cracks tend to avoid the tubules and collagen fibers and propagate away from them. The toughness under wet and dry conditions, however, is not that different as the toughening induced by deflected crack paths in dry scales is offset by the increased "plasticity" of the wet scales, which acts to enhance their ductility.

Appendix A. Figures with essential colour discrimination

Certain figures in this article, particularly Figs. 2, 8, 12, 16 and 18, are difficult to interpret in black and white. The full colour images can be found in the on-line version, at http://dx.doi.org/10.1016/j.actbio.2012.12.026.

References

[1] Burdak VD, editor. Functional morphology of scale cover in fish. Kiev: Naukova Dumka; 1979 [in Russian].

[2] Marino Cugno Garrano A, La Rosa G, Zhang D, Niu N, Tay FR, Majd H, et al. On the mechanical behavior of scales from *Cyprinus carpio*. J Mech Behav Biomed Mater 2012;7:17–29.

[3] Song JH, Ortiz C, Boyce MC. Threat-protection mechanics of an armored fish. J Mech Behav Biomed Mater 2011;4:699–712.

[4] Meyers MA, Lin YS, Olevsky EA, Chen P-Y. Battle in the Amazon: arapaima versus piranha. Adv Eng Mater 2012;14:279–88.

[5] Zhu D, Ortega CF, Motamedi R, Szewciw L, Vernerey F, Barthelat F. Structure and mechanical performance of a "modern" fish scale. Adv Eng Mater 2012;14:185–94.

[6] Yang W, Chen IH, Gludovatz B, Zimmermann EA, Ritchie RO, Meyers MA. Natural flexible dermal armor. Adv Mater 2013;25:31–48.

[7] Smith MM, Hobdell MH, Miller WA. The structure of the scales of *Latimeria chalumnae*. J Zool Lond 1972;167:501–9.

[8] Williamson WC. On the microscopic structure of the scales and dermal teeth of some ganoid and placoid fish. Philos Trans R Soc 1849;1:435–75.

[9] Ikoma T, Kobayashi H, Tanaka J, Walsh D, Mann S. Microstructure, mechanical and biomimetic properties of fish scales from *Pagrus major*. J Struct Biol 2003;142:327–33.

[10] Torres FG, Troncoso OP, Nakamatsu J, Grande CJ, Gomez CM. Characterization of the nanocomposite laminate structure occurring in fish scales from *Arapaima gigas*. Mater Sci Eng C 2008;28:1276–83.

[11] Lin YS, Wei CT, Olevsky EA, Meyers MA. Mechanical properties and the laminate structure of *Arapaima gigas* scales. J Mech Behav Biomed Mater 2011;4:1145–56.

[12] Bruet BJF, Song JH, Boyce MC, Ortiz C. Materials design principles of ancient fish armour. Nature 2008;7:748–56.

[13] Ørvig T. Phylogeny of tooth tissues: evolution of some calcified tissues in early vertebrates. In: Miles AE, editor. Structural and chemical organization of teeth. New York: Academic Press; 1967. p. 45–110.

[14] Meunier FJ. Recherches histologiques sur le squelette dermique des Polypteridae. Arch Zool Exp Gen 1980;122:279–95.

[15] Han L, Wang LF, Song JH, Boyce MC, Ortiz C. Direct quantification of the mechanical anosisotropy and fracture of an individual exoskeleton layer via uniaxial compression of micropillars. Nano Lett 2011;11:3868–74.

[16] Chen P-Y, Schirer J, Simpson A, Nay R, Lin Y-S, Yang W, et al. Predation versus protection: fish teeth and scales evaluated by nanoindentation. J Mater Res 2012;27:100–12.

[17] Koester KJ, Ager JW, Ritchie RO. How tough is human bone? In situ measurements on realistically short cracks. Nat Mater 2008;7:672–7.

[18] American Society for Testing and Materials. ASTME-1820-11: standard test method for measurement of fracture toughness. Annual book of ASTM standards. American Society for Testing and Materials: Philadelphia, PA; 2011.

[19] Kinney JH, Haupt DL, Nichols MC, Breunig TM, Marshall Jr GW, Marshall SJ. The X-ray tomographic microscope: three-dimensional perspectives of evolving microstructures. Nucl Instrum Methods Phys Res Sect A 1994;347:480–6.

[20] Parry DAD, Barnes GRG, Craig AS. A comparison of the size distribution of collagen fibrils in connective tissues as a function of age and a possible relation between fibril size distribution and mechanical properties. Proc R Soc Lond 1978;203:305–21.

[21] Bloom W, Fawcet DW. A textbook of histology. 9th ed. Philadelphia, PA: Saunders; 1968.

[22] Vernerey FJ, Barthelat F. On the mechanics of fish scale structure. Int J Solids Struct 2010;47:2268–75.

[23] Nalla RK, Balooch M, Ager JW, Kruzic JJ, Kinney JH, Ritchie RO. Effects of polar solvents on the fracture resistance of dentin: role of water hydration. Acta Biomater 2005;1:31–43.

[24] Gautieri A, Vesentini S, Redaelli A, Buehler MJ. Hierarchical structure and nanomechanics of collagen microfibrils from the atomistic scale up. Nano Lett 2011;11:757–66.

[25] Jackson AP, Vincent JFV, Turner RM. The mechanical design of nacre. Proc R Soc Lond B 1988;234:415–40.

[26] Rho J-Y, Pharr GM. Effects of drying on the mechanical properties of bovine femur measured by nanoindentation. J Mater Sci Mater Med 1999;10:485–8.

[27] Meyers MA, Chawla KK. Mechanical behavior of materials. Englewood Cliffs, NJ: Prentice-Hall; 1999.

[28] Koester KJ, Ager JW, Ritchie RO. The effect of aging on crack-growth resistance and toughening mechanisms in human dentin. Biomaterials 2008;29: 1318–28.